Available online at www.sciencedirect.com
ScienceDirect
C. R. Physique 10 (2009) 140–147
COMPTES RENDUS PHYSIQUE

Laser acceleration of particles in plasmas / Accélération laser de particules dans les plasmas

Laser-driven electron acceleration in plasmas with few-cycle pulses

Laszlo Veisz [a,*], Karl Schmid [a,b], Franz Tavella [a,1], Sofia Benavides [a], Raphael Tautz [a], Daniel Herrmann [a], Alexander Buck [a], Bernhard Hidding [c], Andrius Marcinkevicius [a,2], Ulrich Schramm [d], Michael Geissler [e], Jürgen Meyer-ter-Vehn [a], Dietrich Habs [b], Ferenc Krausz [a,b]

[a] *Max-Planck-Institut für Quantenoptik, Hans-Kopfermann-Strasse 1, 85748 Garching, Germany*
[b] *Ludwig-Maximilians-Universität München, Am Coulombwall 1, 85748 Garching, Germany*
[c] *Heinrich-Heine-Universität Düsseldorf, 40225 Düsseldorf, Germany*
[d] *Forschungszentrum Dresden-Rossendorf e. V., Bautzner Landstrasse 128, 01328 Dresden, Germany*
[e] *Queen's University Belfast, Belfast BT7 1NN, UK*

Available online 25 April 2009

Abstract

We report on laser-driven electron acceleration with 8 fs, i.e. three optical cycles, pulse duration and 40 mJ energy. Theory and numerical simulations predict that this experimentally unexplored parameter range is relevant for laser wake-field acceleration. The electron spectra produced are monoenergetic with a peak up to 50 MeV and free of low-energy electrons with thermal spectrum. The electron beam has a typical divergence of 5–10 mrad. The accelerator is routinely operated at 10 Hz and correspondingly it is a promising source for several applications. ***To cite this article: L. Veisz et al., C. R. Physique 10 (2009).***

Résumé

Accélération laser d'électrons dans les plasmas à l'aide d'impulsions formées de quelques cycles. On présente l'accélération laser d'électrons à l'aide d'implusions laser de 8 fs, ce qui représente 3 cycles optiques, et de 40 mJ seulement. La théorie et les simulations numériques prédisent que ce domaine vierge expérimentalement est pertinent pour l'accélération laser par champ de sillage. Le spectre des électrons produit est monoénergétique avec un pic atteignant 50 MeV et exempt d'une composante thermique de basse énergie. Le faisceau d'électrons a typiquement une divergence de 5–10 mrad. L'accélération se fait à 10 Hz de façon routinière et apparaît donc comme une source prometteuse pour diverses applications. ***Pour citer cet article : L. Veisz et al., C. R. Physique 10 (2009).***

Keywords: Laser-driven electron acceleration; Bubble regime; Monoenergetic; Ultrashort pulse

Mots-clés : Accélération laser d'électrons ; Régime de la bulle ; Monoénergétique ; Impulsion ultra-courte

* Corresponding author.
E-mail address: laszlo.veisz@mpq.mpg.de (L. Veisz).
[1] Present address: Deutsches Elektronensynchrotron DESY/HASYLAB, Notkestrasse 85, 22607 Hamburg, Germany.
[2] Present address: IMRA America Inc., 1044 Woodridge Avenue, Ann Arbor, MI 48105, USA.

1631-0705/$ – see front matter
doi:10.1016/j.crhy.2009.03.014

1. Introduction

Laser-driven plasma waves were proposed as compact electron accelerators [1] owing to their ability to produce longitudinal accelerating fields several orders of magnitude higher than those attainable in conventional accelerators. This process is called laser wake-field acceleration and a promising implementation relies on "broken" plasma waves. In this regime the laser intensity is so large that the generated plasma wave breaks directly behind the pulse and some electrons of the background plasma are injected into this first period of the plasma wave and are accelerated. Numerical studies [2–4] have shown that the accelerated electrons emerge from the plasma as monoenergetic electron bunches with relativistic energy and few-femtosecond duration. Under ideal conditions, the driving laser pulse has relativistic intensity ($>10^{18}$ W/cm^2) and a duration and diameter that are matched to the plasma density. This means that ideally a laser pulse is required that has a length of equal to or less than half the plasma wavelength $\lambda_p/2 \approx \pi c/\omega_p$, and a focal diameter of $\approx\lambda_p$. Here $\omega_p = \sqrt{n_e e^2/(\epsilon_0 m_e)}$ is the plasma frequency and e, m_e, n_e electron charge, mass, and density, respectively. In this case, the laser pulse is so intense that its ponderomotive force pushes free electrons transversally out of its path, leaving the positively charged ions behind. The electrons are pulled back to the axis by the electrical field created by charge separation after a propagation length comparable to the plasma wavelength. In that way they form a cavity which is void of electrons and is trailing the laser pulse, dubbed a "bubble". This structure constitutes a highly anharmonic plasma wave that propagates with a phase velocity equal to the group velocity of the laser pulse and breaks down completely after the first (few) period(s) of its oscillation. A fraction of the returning electrons is injected and trapped in the bubble and accelerated by its ultra-strong longitudinal electric field, producing relativistic electron bunches with narrow-band energy spectra [5,6].

In order to reach the intensities required for this scheme with laser pulses of typical durations between 30 and 80 fs and matched spot size, pulse energies in the multi-Joule range are required. This restricts the acceleration regime to rather large lasers or requires additional nonlinear self-modulation of the pulse in the plasma. In the latter case, monoenergetic electron acceleration is preceded by a nonlinear laser–plasma interaction including relativistic self-focusing and temporal modulation of the laser pulse, which transforms the laser pulse into the required domain [7]. In the last few years, many experiments concerning laser-generated monoenergetic electron beams have been conducted, from the proof-of-principle in 2004 [8–13], to follow-up experiments that shed light on important aspects of the mechanism [14–16], employed additional laser-guiding structures to reach electron energies of up to 1 GeV [17–19] and improved the shot-to-shot reproducibility by controlling the injection process [20] or stabilizing the gas target [21]. However all those experiments were conducted with similar laser parameters, using pulses with durations of 30–80 fs necessitating pulse energies in the 1 J range and also relying to different extents on self-modulation and self-shortening in order to reach intensities high enough for wave breaking and monoenergetic electron acceleration to take place.

Analytical scaling laws [3–5] and our simulations, [22], indicate that for laser pulses shorter than 10 fs at typical plasma densities, a self-modulation-free acceleration regime can be accessed delivering moderate electron energies and large bunch charge with less than 100 mJ pulse energy. Here we demonstrate mono-energetic electron acceleration in this new laser-parameter range, employing for the first time few-cycle laser pulses to this end. A laser pulse duration of 8 fs allows to reach the desired acceleration process with only 40 mJ energy [23].

2. Experimental setup

In our experiments we used LWS-10 (Light Wave Synthesizer-10), the world's first multi-TW sub-10-fs light source. It is based on non-collinear optical parametric chirped pulse amplification (OPCPA). The seed for the two OPCPA stages is generated by a commercial Ti:sapphire front-end [24]; subsequently its output is spectrally broadened in a neon-filled hollow-core fiber and stretched to 30 ps duration by a negative dispersion stretcher. After parametric amplification in two BBO crystals, bulk glass blocks and chirped mirrors are used to compress the pulses. The pump pulses for the OPCPA are generated by a frequency doubled Nd:YAG amplifier that is seeded by the same oscillator as the front end, providing all-optical synchronization of pump and seed laser. The pump laser delivers 80 ps pulses with up to 600 mJ at a wavelength of 532 nm. During the experiments the system produced pulses with 50-mJ energy, 8 fs duration and spectra covering the range of 700–980 nm at 10-Hz repetition rate. Due to losses in the vacuum beamline connecting laser and experiment, the energy on target was only 40 mJ. An adaptive mirror and a wavefront sensor in closed loop configuration are used to correct wavefront aberrations and also allow to modify the focal spot diameter without changing the focusing optics in the experiment [25].

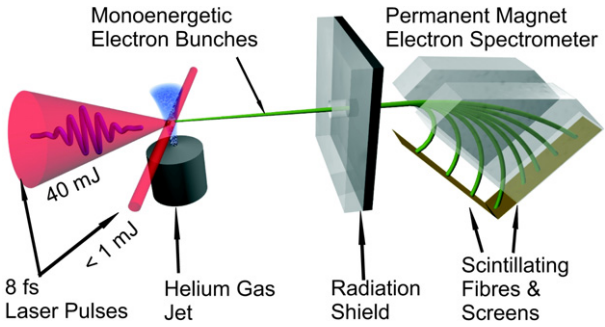

Fig. 1. Schematic illustration of the experiment. The 8-fs laser pulses are split into a driver beam with 40-mJ energy and a weak probe beam with less than 1 mJ energy. The driver beam is focused onto a helium jet with electron densities between 10^{18} to 10^{20} cm^{-3}. The electron beam emerging from the laser–plasma interaction is characterized by a permanent magnet electron spectrometer.

The laser pulses were focused by a gold-coated F/6 off-axis parabola onto a helium gas jet (see Fig. 1) to a spot diameter of 6 μm FWHM, yielding a peak intensity of 1.2×10^{19} W/cm^2 or a normalized vector potential $a_0 \approx 2.4$. The helium interaction medium is provided either by a flat-top supersonic gas jet with a diameter of 300 μm generated by a Laval nozzle or by a subsonic gas jet with a Gaussian-shaped density profile produced by a cylindrical nozzle with a diameter of 400 μm. Reference measurements were made also with a 150 μm diameter Laval nozzle. The plasma density can be varied between 10^{18} and 10^{20} cm^{-3}, optimal conditions for our current laser parameters are obtained with an electron density of 2×10^{19} cm^{-3}. A density change of $\pm 10\%$ resulted in significantly increased fluctuations in the electron beam properties. The laser-generated plasma channel is imaged transversally by a long-object-distance microscope objective onto a CCD camera, allowing high resolution measurements of channel diameter and length. In addition, a weak probe beam can be coupled into the side-view imaging system for assisting in the alignment of the nozzle to the focal spot and for plasma diagnostics.

The electron energy spectrum is measured by a high resolution focusing permanent magnet spectrometer suitable for analyzing electrons in the range of 2–400 MeV. It consists of a 30-cm × 40-cm focusing permanent magnet combined with a yoke, having a magnetic field of 1 T over a gap of 5 cm and uses either 600 highly-sensitive scintillating fibers coupled to a 16 bit CCD camera or scintillating screens (Kodak Lanex) imaged to a 12 bit CCD-camera as detection system, allowing simultaneous measurement of energy spectrum and divergence. The scintillating screens have lower sensitivity, but higher energy resolution than the fibers. Lanex and fibers were cross-calibrated against an image plate [26]. Unfortunately, due to subsequent changes in the detection system, the measured charge-values are accurate only to a factor of 2. Additionally a smaller spectrometer was used to analyze electrons within low to moderately-relativistic energies of 100 keV–13 MeV [27].

3. Results and discussion

Typical spectra of electron beams emerging from the plasma accelerator using the 400 μm cylindrical nozzle are shown in Fig. 2a. The displayed spectra comprise a very low amount of thermal electrons at low energies and pronounced monoenergetic peaks between 13 and 23 MeV while the charge in the peak is on the order of 10 pC. The FWHM spectral bandwidth is in the 3–10% range. The small spectrometer was applied to investigate the low energy part of the electron spectrum below 2 MeV. Typical results are plotted in Fig. 2b. Monoenergetic peaks are present at 4.3 and 9.8 MeV and there is no sign of a background exponential electron spectrum down to 100 keV energy.

Fig. 3 shows raw data and calibrated lineouts of a shot captured on the scintillating screen in the spectrometer. The spectrum shows a monoenergetic peak at 24.6 MeV with 3.3% relative energy spread – FWHM, a transversal divergence of 6.3 mrad – FWHM – and a charge of approximately 3 pC. In the raw data image two weak features at higher energies are visible, they probably stem from injection and acceleration in different plasma wave troughs. This effect was also observed in our simulations.

The spectrum of the highest observed electron energy with 40 mJ laser energy is in Fig. 4 and has a 50 MeV quasi-mono-energetic peak. The number of electrons in the Maxwellian tail was comparable to the number of electrons in the peak, which is still a relatively small background when compared to earlier instances of laser–plasma-generated electron bunches.

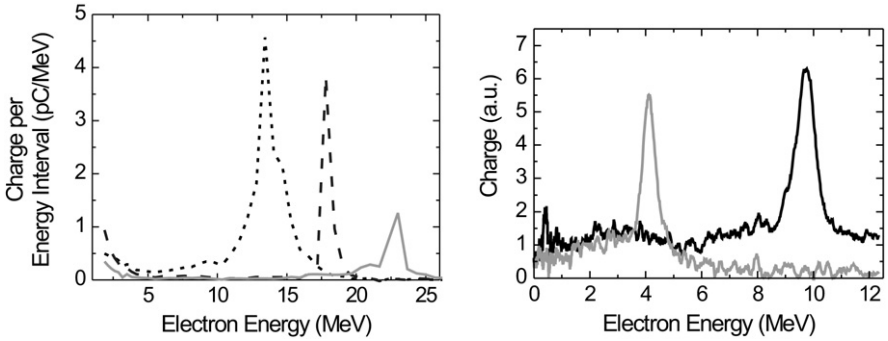

(a) (b)

Fig. 2. Typical spectra of monoenergetic electron beams with very low thermal background. Panel (a) shows three spectra with mean energies of 13.4, 17.8 and 23 MeV. The charge in the peaks is approximately 10, 3.5 and 1.6 pC respectively. Panel (b) shows the results obtained using a smaller spectrometer down to 100 keV electron energy. It confirms the low amount of exponential electrons. These spectra were obtained with the cylindrical subsonic 400 μm gas jet.

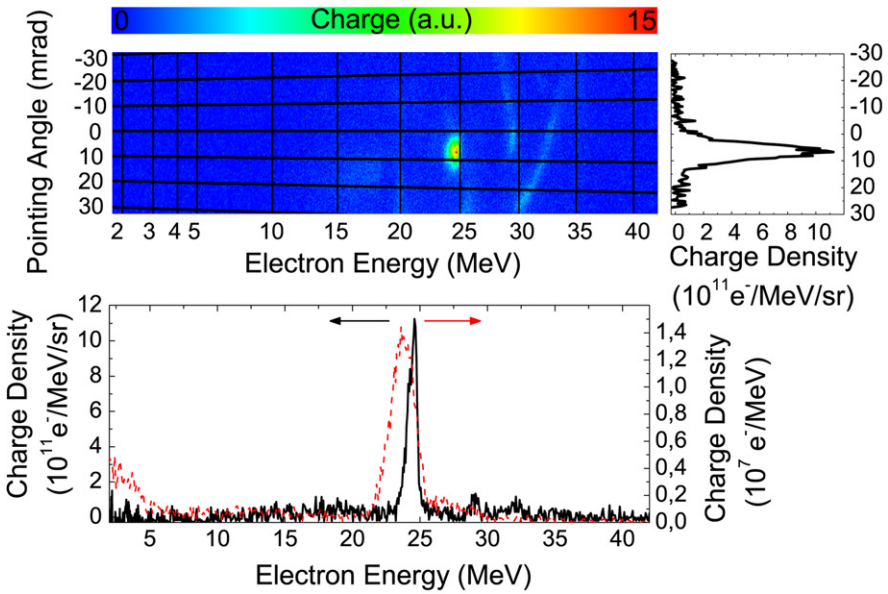

Fig. 3. Electron spectrum and transverse beam size obtained with a scintillating screen placed in the electron spectrometer and imaged onto a CCD camera. Shown is the raw image, together with calibrated lineouts along the energy axis (lower plot) and the transversal axis (right side). The displayed result was obtained with a 300 μm supersonic gas jet and exhibits a monoenergetic peak at 24.6 MeV with 3.3% energy spread – FWHM, a divergence of 6.3 mrad – FWHM – and a charge of 3 pC. Also shown is the simulated electron spectrum (red, dashed), which is in very good agreement with the experimental result.

To investigate the acceleration at lower intensities the beam diameter was decreased on the focusing parabola by the adaptive mirror leading to an effective F/11 focusing. Under these circumstances the beam was focused to a spot diameter of 10.7 μm and a peak intensity of 3.8×10^{18} W/cm^2 or a normalized vector potential $a_0 = 1.3$. The probability of generating mono-energetic electrons decreased significantly and the number of shots producing multiple bunches increased. In contrary to the F/6 focusing, where a main peak and sometimes 1–2 weak secondary peaks were obtained, electron spectra containing even 5–6 bunches with comparable charges have been observed as shown in Fig. 5. Similar multiple bunching effects were simulated and interpreted as multiple injection in one plasma trough as well as injection in different plasma wave periods [28]. The intensity was also varied by changing laser pulse duration and energy. The electron acceleration process was very sensitive to the pulse length and we have not observed electrons if the pulse was longer than 13–14 fs. Similarly, as the intensity was changed by gradual reduction

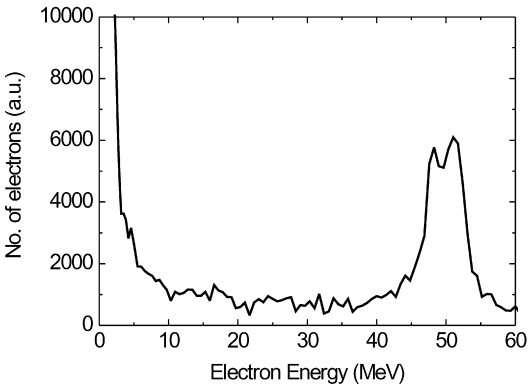

Fig. 4. 50 MeV quasi-monoenergetic electron spectrum. This is the highest electron energy observed still with a relative low thermal background. This spectrum was obtained with the cylindrical – subsonic – 400 μm gas jet and 40 mJ laser energy.

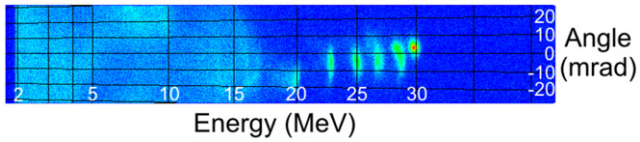

Fig. 5. Multiple electron bunches with F/11 focusing. This spectrum was obtained with the supersonic 300 μm gas jet and 40 mJ laser energy.

of the laser pulse energy it resulted in rapid increase of fluctuations of the electron beam properties, with acceleration ceasing completely for pulse energies below 25–30 mJ.

The side-view imaging of the interaction region revealed a weakly scattering, channel-like structure with a length of approximately 100–120 μm, which is approximately equal to the Rayleigh range of the laser beam, and a diameter of approximately 5 μm. Strong scattering, indicative of self-modulation observed in experiments with longer laser pulses, was not observed. Since no pronounced structure of the channel was measured the point of injection could not be determined. The measured channel length and electron energies of 10–30 MeV imply an average longitudinal accelerating gradient of 0.1–0.3 TeV/m, if it is assumed that acceleration takes place over the full channel length. Similar minimal gradient values were obtained from the reference measurements with the 150 μm diameter Laval nozzle. This gradient is also in good agreement with previously reported values [29] as well as with our simulations.

An interesting feature of the mono-energetic energy spectra is the apparently low number of low-energy "thermal" electrons. These thermal electrons show up in the electron spectrum with an exponentially decaying energy distribution. Correspondingly a temperature may be assigned to these electrons which typically lies between 1 and 10 MeV, see for example [29–31]. We confirmed the low amount of thermal electrons – sometimes even below detection limit – down to energies of 100 keV by introducing an electron spectrometer optimized for the energy range of 100 keV to 13 MeV, see Fig. 2b. We note that comparison to earlier experiments is difficult due to the fact that in the majority of the cases the electron spectrum was not measured down to the energy range of the thermal electrons of a few MeV. The low thermal background also leads to a low dose of gamma radiation generated by the electron beam, which was about thousand times less than with a 45 fs laser near the vacuum chamber. This, together with the low gas load owing to the small nozzles, enabled us to routinely operate the electron accelerator at 10-Hz repetition rate using ordinary vacuum pump systems, which makes this electron source attractive for a number of applications. It remains to be verified whether the low background is preserved with increased laser pulse energy – which would mean that this is a property of the pure "bubble regime" – or not.

Both types of gas jets yield electron beams of comparable properties, but the supersonic jet performs significantly better in terms of shot-to-shot reproducibility of the parameters of the accelerated electron bunch. This can be attributed to the steep density gradients at the border of the jet and the uniform gas density inside the interaction volume.

To gain more insight into the details of the acceleration process, we performed numerical simulations with the 3-dimensional particle-in-cell (3D-PIC) code ILLUMINATION [22]. The co-moving simulation box represents a

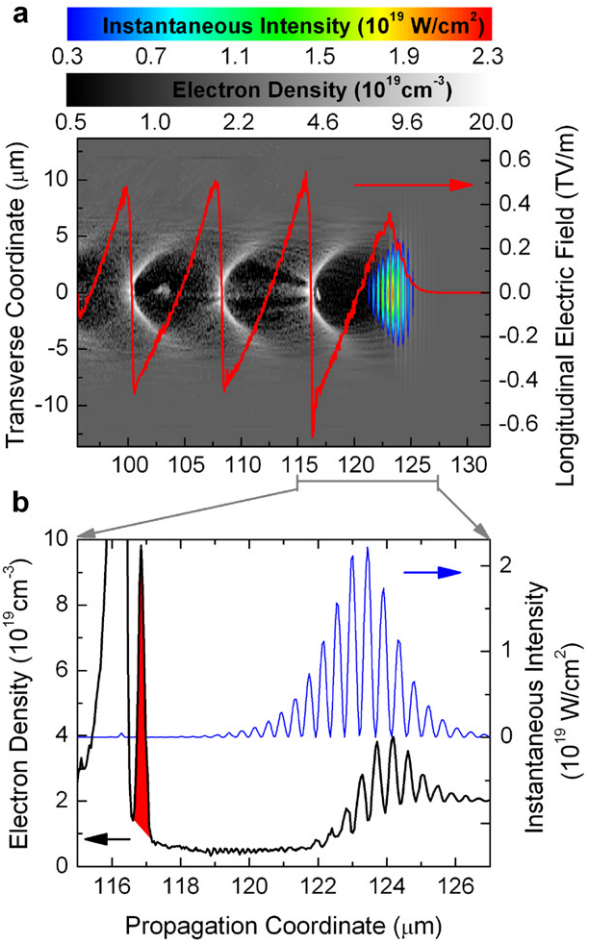

Fig. 6. Simulation results showing the physical state of the system after the laser pulse has traveled a distance of 125 μm inside the plasma. Panel (a) shows the electron density (gray-scale plot) and the instantaneous laser intensity (false-color diagram). The laser intensity plot is clipped along the contour line where the intensity drops by a factor of $1/e^2$ with respect to its peak value. It is evident that the laser pulse fits within the bubble radius. The red line shows the longitudinal accelerating field caused by charge separation in the bubble (forward-directed field has positive value). The field strength is about 0.45 TV/m at the location of the bunch. Panel (b) plots lineouts of electron density and instantaneous laser intensity along the optical axis of the laser beam at center of the simulation box. The injected electron bunch – red – contains 4.5 pC charge and has an order of magnitude higher density than the background plasma.

volume of $27 \times 27 \times 36$ μm – z is the propagation axis – with a grid size of 94/94/47 nm. The plasma is treated as fully (pre-)ionized with one macro-particle per cell and immobile ions as a charge neutralizing background. It is modeled with a uniform transversal density distribution, whereas in the longitudinal direction a 120-μm broad flat-top profile, matching the experimentally determined channel length, with an electron density of 2×10^{19} cm^{-3} terminated by exponential gradient slopes, are assumed. The $1/e$ scale length of the entrance gradient is 5 μm, just to avoid numerical problems with a steep gradient. The exit gradient was chosen as 30 μm to match the experimental conditions. The simulations have been performed with a time step of 0.1 fs, using the following laser parameters: pulse duration: 8.5 fs (FWHM), Gaussian beam waist: 6 μm, pulse energy: 38 mJ, and carrier laser wavelength: 800 nm.

Fig. 6a shows a snapshot of the electron density distribution, laser intensity and longitudinal electrical field of the plasma accelerator after the laser pulse has traveled 125 μm across the 155-μm-thick gas jet. The typical characteristics of laser-driven electron acceleration as the strongly-driven plasma wave, the forming electron voids – "bubbles" – trailing the laser pulse, as well as the breaking of this wave are obvious in this figure. The laser pulse, clipped at the $1/e^2$-contour, clearly fits into the first half of the bubble and does not overlap with the accelerated electron bunch. Fig. 6b shows line-outs of instantaneous laser intensity and electron density along the optical axis of the laser beam in a propagation interval confining the laser pulse and the first bubble behind it. The laser pulse expels approximately 75%

of the free electrons in the vicinity of the propagation axis, leaving a depleted trough behind. The expelled electrons swing back to the axis forming the prominent density peak at the back of the bubble. Some of the returning electrons are then scattered into the bubble by the repulsing field of that density peak. Along some propagation distance these injected electrons accumulate in the bubble, forming a dense electron bunch – shown in red – that is trapped and accelerated. The accelerating electrical field is induced by the charge separation of the strong electron density peak at the bubble vertex and by the positively charged ions inside the bubble. A plot of the longitudinal electrical field on axis is given in Fig. 6a – red line. At the location of the bunch, the longitudinal electric field amounts to approximately 0.45 TV/m and is hardly perturbed by beam loading effects – the field induced by the bunch itself, in principle permitting further charge accumulation in the beam. The electron spectrum after the electron bunch left the plasma and propagated several 100 μm into the surrounding vacuum is given in Fig. 3b with the dashed red line. It shows a monoenergetic peak at 24 MeV, which implies an effective acceleration length of about 60 μm for the accelerating field of 0.45 TV/m. The electron bunch emerging from the plasma carries a charge of about 4.5 pC, has a duration on the order of 1 fs and is accompanied by a small exponential background. The ultrashort electron bunch duration is approximately preserved within the range of simulated propagation extending several 100 micrometers behind the gas jet.

Our simulations indicate that the laser intensity in our case is just high enough to produce self-injection but still low enough to produce a wake field extending over several oscillations. Indeed the simulations show that our current laser parameters are close to the threshold below which no self-injection and formation of a stable accelerating structure occurs any more [22]. This is in good agreement with both the analytic theory of bubble acceleration [5], which – for our pulse duration – predicts the onset of the process at pulse energies of about 25 mJ, and the experimental result that the lower limit was 25–30 mJ. This implies that with our current on-target energy of 40 mJ we operate the bubble accelerator very close to the boundary of its operational regime. Higher driving pulse energies should not only improve stability but – according to our simulations – also dramatically increase the laser-to-electron energy conversion efficiency, from currently $\sim$1% to up to 20%. Furthermore the simulations show that the laser pulse is rapidly depleted and therefore looses its ability to sustain a stable bubble already after 250 μm propagation. To verify this an extremely small Laval-nozzle with only 150 μm exit diameter was used to produce a gas target with a length shorter than the depletion length of the laser, which led to an improved stability but also to lower electron energies.

4. Summary

We successfully applied a novel light source, an optical parametric chirped pulse amplifier generating 8 fs pulse duration, corresponding to three optical cycles, and 40 mJ energy pulses to laser-driven electron acceleration. Small 150–400 μm diameter supersonic Laval and subsonic cylindrical nozzles were used to provide the He interaction medium. Monoenergetic electron bunches in the multi-10 MeV range up to 50 MeV energy and with narrow (3–10% FWHM) spectral bandwidth were observed with approximately 10 pC charge and 5 to 10 mrad FWHM divergence. Very low amount of or even in some cases no thermal background electrons were observed leading to low secondary x-ray radiation. The electron accelerator is routinely operated at 10 Hz due to the low radiation and the low gas load from small nozzles. Simulations support the experimental findings and indicate 1 fs electron bunch duration. The results make few-cycle-laser-driven electron acceleration appear a promising concept for producing relativistic, monoenergetic electron bunches with ultrashort duration. This electron source is perfectly suited for many applications including time-resolved laser-pump electron-probe experiments and seeding of wake-field acceleration stages. The OPCPA light source has the potential to improve the driver pulse repetition rate and pulse energy significantly and so further broaden the range of applications.

Acknowledgements

We would like to thank Stefan Karsch for many helpful discussions as well as for help with the experimental setup. This work was supported by DFG-Project Transregio TR18 by the Association EURATOM – Max-Planck-Institut fuer Plasmaphysik and by The Munich Centre for Advanced Photonics (MAP).

References

[1] T. Tajima, D. Dawson, Laser electron accelerator, Phys. Rev. Lett. 43 (1979) 267.

[2] A. Pukhov, et al., Laser wake field acceleration: the highly non-linear broken-wave regime, Appl. Phys. B 74 (2002) 355.
[3] W. Lu, et al., Nonlinear theory for relativistic plasma wakefields in the blowout regime, Phys. Rev. Lett. 96 (2006) 165002.
[4] F.S. Tsung, et al., Simulation of monoenergetic electron generation via laser wakefield accelerators for 5–25 TW lasers, Phys. Plasmas 13 (2006) 056708.
[5] S. Gordienko, A. Pukhov, Scalings for ultrarelativistic laser plasmas and quasimonoenergetic electrons, Phys. Plasmas 12 (2005) 043109.
[6] A. Pukhov, S. Gordienko, Bubble regime of wake field acceleration: similarity theory and optimal scalings, Philos. Trans. R. Soc. A 364 (2006) 623.
[7] J. Faure, et al., Observation of laser-pulse shortening in nonlinear plasma waves, Phys. Rev. Lett. 95 (2005) 205003.
[8] J. Faure, et al., A laser–plasma accelerator producing monoenergetic electron beams, Nature 431 (2004) 541.
[9] V. Malka, et al., Monoenergetic electron beam optimization in the bubble regime, Phys. Plasmas 12 (2005) 056702.
[10] C.G.R. Geddes, et al., High quality electron beams from a laser wakefield accelerator using plasma-channel guiding, Nature 431 (2004) 538.
[11] C.G.R. Geddes, et al., Production of high-quality electron bunches by dephasing and beam loading in channeled and unchanneled laser plasma accelerators, Phys. Plasmas 12 (2005) 056709.
[12] S.P.D. Mangles, et al., Monoenergetic beams of relativistic electrons from intense laser plasma interactions, Nature 431 (2004) 535.
[13] S.P.D. Mangles, et al., The generation of mono-energetic electron beams from ultrashort pulse laser–plasma interactions, Philos. Trans. R. Soc. A 364 (2006) 663.
[14] T. Hosokai, et al., Observation of strong correlation between quasimonoenergetic electron beam generation by laser wakefield and laser guiding inside a preplasma cavity, Phys. Rev. E 73 (2006) 036407.
[15] A. Maksimchuk, et al., Studies of laser wakefield structures and electron acceleration in underdense plasmas, Phys. Plasmas 15 (2008) 056703.
[16] B. Hidding, et al., Generation of quasimonoenergetic electron bunches with 80-fs laser pulses, Phys. Rev. Lett. 96 (2006) 105004.
[17] W.P. Leemans, et al., GeV electron beams from a centimeter-scale accelerator, Nat. Phys. 2 (2006) 696.
[18] T.P. Rowlands-Rees, et al., Laser-driven acceleration of electrons in a partially ionized plasma channel, Phys. Rev. Lett. 100 (2008) 105005.
[19] S. Karsch, et al., GeV-scale electron acceleration in a gas-filled capillary discharge waveguide, New J. Phys. 9 (2007) 415.
[20] J. Faure, et al., Controlled injection and acceleration of electrons in plasma wakefields by colliding laser pulses, Nature 444 (2006) 737.
[21] J. Osterhoff, et al., Generation of stable, low-divergence electron beams by laser-wakefield acceleration in a steady-state-flow gas cell, Phys. Rev. Lett. 101 (2008) 085002.
[22] M. Geissler, et al., Bubble acceleration of electrons with few-cycle laser pulses, New J. Phys. 8 (2006) 186.
[23] K. Schmid, et al., Few-cycle laser-driven electron acceleration, Phys. Rev. Lett. 102 (2009) 124801.
[24] Femtolasers GmbH, Femtopower Compact Pro.
[25] F. Tavella, et al., Dispersion management for a sub-10-fs, 10 TW optical parametric chirped-pulse amplifier, Opt. Lett. 32 (2007) 2227.
[26] B. Hidding, et al., Novel method for characterizing relativistic electron beams in a harsh laser–plasma environment, Rev. Sci. Instrum. 78 (2007) 083301.
[27] C. Gahn, et al., Multi-MeV electron beam generation by direct laser acceleration in high-density plasma channels, Phys. Rev. Lett. 83 (1999) 4772.
[28] A. Oguchi, et al., Multiple self-injection in the acceleration of monoenergetic electrons by a laser wake field, Phys. Plasmas 15 (2008) 043102.
[29] C.-T. Hsieh, et al., Tomography of injection and acceleration of monoenergetic electrons in a laser-wakefield accelerator, Phys. Rev. Lett. 96 (2006) 095001.
[30] A. Yamazaki, et al., Quasi-monoenergetic electron beam generation during laser pulse interaction with very low density plasmas, Phys. Plasmas 12 (2005) 093101.
[31] S. Masuda, et al., Energy scaling of monoenergetic electron beams generated by the laser-driven plasma based accelerator, Phys. Plasmas 14 (2007) 023103.